Inorg. Chem. **2009**, *48*, 1346−1355

$R_3Au_{6+x}Al_{26}T$ (R = Ca, Sr, Eu, Yb; T = Early Transition Metal): a Large Family of Compounds with a Stuffed $BaHg_{11}$ Structure Type Grown from Aluminum Flux

Susan E. Latturner,[†] Daniel Bilc,[‡] S. D. Mahanti,[‡] and Mercouri G. Kanatzidis*[,§]

Department of Chemistry, Northwestern University, Evanston, Illinois 60208, Department of Chemistry, Florida State University, Tallahassee, Florida 32306, and Department of Physics, Michigan State University, East Lansing, Michigan 48824

Received June 25, 2008

A collection of new quaternary intermetallic compounds with a cubic, stuffed $BaHg_{11}$ structure type has been synthesized by the combination of a divalent rare earth or alkaline earth metal R, an early transition metal T, and gold in an excess of molten aluminum. Structural characterization of these $R_3Au_{6+x}Al_{26}T$ compounds by powder and single crystal X-ray diffraction indicates that the unit cell varies with the radii of the early transition metal T and the rare earth/alkaline earth R as expected. The element T (where T = group 4, 5, 6, and 7 element) appears to be responsible for the stabilization of up to 43 different members of the $R_3Au_{6+x}Al_{26}T$ family of compounds. Varying amounts of disorder and trends in partial occupancies of the Au stuffed site—the site that is vacant in the parent compound $BaHg_{11}$—are also indicated by the diffraction studies of this family of compounds. Magnetic susceptibility data reveals that the transition metal atoms in these materials do not possess local magnetic moments. For the magnetic rare earth containing materials, the europium compounds undergo a ferromagnetic transition at 10 K, and the ytterbium analogues show mixed valent behavior. Band structure calculations also support a mixed valent state for Yb in these compounds.

Introduction

Elements such as lanthanides, transition metals, and silicon are often added to aluminum alloys to optimize their properties. Many of the changes in the observed behavior are due to the formation of as yet unexplored multinary intermetallics within the aluminum matrix; investigation of these adventitious compounds is necessary to understand and control the characteristics of the bulk alloy.[1] Aluminum-rich intermetallics often possess complex structures composed of a variety of clusters and feature prominently in the fields of metallic glasses and quasicrystals.[2] Exploratory synthesis in molten aluminum is being carried out, first, to discover new materials with novel structures, bonding, and properties and, second, to investigate the adventitious growth of intermetallics in aluminum alloys. Undoubtedly, there seems to exist a wide variety of complex bonding motifs inherent in aluminide phases.

Metal flux chemistry has several advantages, including ready dissolution of many elements, which become reactive well below their melting point. Synthesis can be carried out at low enough temperatures to allow the formation and crystallization of new metastable or kinetically stabilized phases.[3] Aluminum flux research has yielded a wide variety of new compounds such as ternaries $RE_2Al_3Si_2$, $Co_{19}Al_{45}Si_{10-x}$, and $REAu_3Al_7$, and quaternaries $RENiAl_4Ge_2$ and $RE_2NiAl_4Ge_2$.[4] The behavior of silicon in molten aluminum has been of particular interest because of the wide use of this element as an additive in alloys. Reaction of silicon with other elements in aluminum flux has yielded a variety of complex aluminides such as $Sm_2Ni(Ni_x$-

* To whom correspondence should be addressed. E-mail: m-kanatzidis@northwestern.edu.
† Florida State University.
‡ Michigan State University.
§ Northwestern University.

(1) (a) Suresh, S.; Mortensen, A.; Needleman, A. *Fundamentals of Metal-Matrix Composites*; Butterworth-Heinemann: Boston, 1993. (b) Mondolfo, L. F. *Aluminum Alloys: Structure and Properties*; Butterworth-Heinemann: Boston, 1979. (c) Jackson, A. G.; Mahajan, Y. R.; Kirchoff, S. D. *Scr. Metall.* **1986**, *20*, 1247.

(2) (a) Steurer, W. *Z. Kristallogr.* **2004**, *219*, 391–446. (b) Tsai, A. P. *MRS Bull.* **1997**, *22*, 43–47. (c) Greer, A. L. *Science* **1995**, *267*, 1947–1953.

(3) Kanatzidis, M. G.; Pottgen, R.; Jeitschko, W. *Angew. Chem., Int. Ed.* **2005**, *44*, 6996.

10.1021/ic801095v CCC: $40.75
Published on Web 01/15/2009

$Si_{1-x})Al_4Si_6$, $RE_4Fe_{2+x}Al_{7-x}Si_8$, and $RE_8Ru_{12}Al_{49}Si_9(Al_xSi_{12-x})$.[5] Expanding on this work to explore the reactivity of third row transition metals, two series of interrelated homologous compounds were formed in reactions containing gold: $Th_2[AuAl_2]_n(Au_xSi_{1-x})Si_2$ and $RE[AuAl_2]_nAl_2(Au_xSi_{1-x})_2$.[6] Both families of structures feature large anti-fluorite $AuAl_2$ slabs capped with silicon.

In this work, synthesis of intermetallics from the combination of a rare earth element, gold, and an early transition metal in molten aluminum was investigated to determine the effect of replacing silicon with electropositive transition metals. While reactions with most of the rare earths produced mixtures of $REAu_3Al_7$ and transition metal aluminides, reactions with europium and ytterbium yielded a quaternary variant of the cubic $BaHg_{11}$ structure, $R_3Au_{6+x}Al_{26}T$ ($0 \leq x \leq 2$). This phase forms with all transition metals T in groups 4−7, and it is also formed when the rare earth elements are replaced by Ca and Sr. The titanium-containing analogues with R = Ca, Sr, and Yb were discussed in an earlier brief communication.[7] This family of compounds (up to 43 members are reported here) which is stabilized by the transition metal T is much broader in scope than originally envisioned and features several modes of disorder, including a variable occupancy stuffed site and a split site that leads to supercell formation in some analogues. The $Yb_3Au_{6+x}Al_{26}T$ compounds have complex magnetic behavior, with the Yb ions showing two kinds of non-integral (Yb^{2+}/Yb^{3+}) valence. To investigate this issue we carried out band structure calculations on an ytterbium-containing model structure.

Experimental Procedure

Synthesis. The $R_3Au_{6+x}Al_{26}T$ compounds were synthesized by combining the elements in a 1:2:15:1 molar ratio. In a nitrogen atmosphere glovebox, 0.5 mmol rare earth or alkaline earth metal (Cerac, 99.99%), 1 mmol gold (1 ounce gold coin, 99.99%), 7.5 mmol aluminum (Cerac, 99.99%), and 0.5 mmol early transition metal (T = group 4 −7 metals, except Tc) were combined in an alumina crucible. This was sealed in a fused silica tube under a vacuum of 10^{-4} Torr. The reaction vessel was heated to 1000 °C in 12 h, held at this temperature for 15 h, then cooled to 860 °C in 1 d. It was annealed at 860 °C for 60 h, then cooled to room temperature in 3 d. The excess aluminum flux was removed by soaking the crucible and contents in 5 M NaOH for 24 h.

Elemental analysis on the products was carried out using a JEOL JSM-35C scanning electron microscope with energy dispersive spectroscopy (EDS) capabilities. Ten to twenty crystals of each analogue were analyzed using a 20 kV accelerating voltage and an accumulation time of 50 s. In most cases the $R_3Au_{6+x}Al_{26}T$ crystals were non-uniformly coated with a reflective reddish-purple film (for R = Yb, Eu) or a dull brown or gold film (for R = Ca, Sr). EDS indicates this film is rich in R and gold; it is possibly a binary such as R_2Au_7, or a degradation product due to leaching of the aluminum in the compound by the NaOH solution. EDS on the interior of these samples indicates a stoichiometry of $R_3Au_{6-7}Al_{20}T$. A slightly low reading for aluminum is not uncommon for this instrument.

X-ray Diffraction. Single crystal X-ray diffraction data for each compound were collected at room temperature on a Bruker AXS SMART CCD diffractometer. Full sphere or hemisphere data collections were carried out for over half of the $R_3Au_{6+x}Al_{26}T$ compounds; for the rest a matrix was collected to determine the symmetry and the unit cell parameters. For the full data sets, data processing was performed using the program SAINT; an absorption correction was applied to the data using the SADABS program.[8] The structure was solved using direct methods and refined with the SHELXTL package of programs.[9] After locating most of the atoms, a split site was indicated by a high peak in the electron density near the partially occupied Au(2) site. This was refined as a partially occupied Al(2) site. The occupancies of Au(2) and Al(2) were observed to sum close to 1 even without restraining; since this makes physical sense, this restraint was applied in the final refinement cycles. Anisotropic refinement of the Al(2) site often leads to unstable refinement, so this atom was refined isotropically. The data collection parameters, atomic positions, and selected bond lengths for three representative $R_3Au_{6+x}Al_{26}T$ compounds are listed in Tables 1, 2, and 3. Additional crystallographic refinement parameters can be found in the Supporting Information. Powder diffraction was carried out on a number of analogues using an INEL powder diffractometer.

Magnetic Susceptibility Measurements. Magnetic susceptibility measurements were carried out with a Quantum Design MPMS SQUID magnetometer at temperatures between 3 and 300 K. For several analogues, EDS-analyzed crystals were ground into powder; this was sealed in kapton tape and placed into the magnetometer. Field cooled and zero field cooled temperature dependence data were collected at 1000 G, and field dependence data were collected at 3 K.

Band Structure Calculations. The electronic structure calculations for $Yb_3Au_7Al_{26}V$ were performed within density functional theory (DFT) using the self-consistent full potential linearized augmented plane wave (LAPW)[10] method implemented in the WIEN 97 code.[11] Because these calculations are not amenable to

(4) (a) Chen, X. Z.; Sieve, B.; Henning, R.; Schultz, A. J.; Brazis, P.; Kannewurf, C. R.; Cowen, J. A.; Crosby, R.; Kanatzidis, M. G. *Angew. Chem., Int. Ed.* **1999**, *38*, 693–696. (b) Wu, X. U.; Latturner, S. E.; Kanatzidis, M. G. *Inorg. Chem.* **2006**, *45*, 5358–5366. (c) Latturner, S. E.; Bilc, D.; Ireland, J.; Kannewurf, C. R.; Mahanti, S. D.; Kanatzidis, M. G. *J. Solid State Chem.* **2003**, *170*, 48–57. (d) Sieve, B.; Chen, X. Z.; Cowen, J. A.; Larson, P.; Mahanti, S. D.; Kanatzidis, M. G. *Chem. Mater.* **1999**, *11*, 2451–2455. (e) Sieve, B.; Trikalitis, P. N.; Kanatzidis, M. G. *Z. Anorg. Allg. Chem.* **2002**, *628*, 1568–1574.

(5) (a) Chen, X. Z.; Sportouch, S.; Sieve, B.; Brazis, P.; Kannewurf, C. R.; Cowen, J. A.; Patschke, R.; Kanatzidis, M. G. *Chem. Mater.* **1998**, *10*, 3202–3211. (b) Sieve, B.; Sportouch, S.; Chen, X. Z.; Cowen, J. A.; Brazis, P.; Kannewurf, C. R.; Papaefthymiou, V.; Kanatzidis, M. G. *Chem. Mater.* **2001**, *13*, 273–283. (c) Sieve, B.; Chen, X. Z.; Henning, R.; Brazis, P.; Kannewurf, C. R.; Cowen, J. A.; Schultz, A. J.; Kanatzidis, M. G. *J. Am. Chem. Soc.* **2001**, *123*, 7040–7047.

(6) (a) Latturner, S. E.; Bilc, D.; Mahanti, S. D.; Kanatzidis, M. G. *Chem. Mater.* **2002**, *14*, 1695–1705. (b) Latturner, S. E.; Kanatzidis, M. G. *Inorg. Chem.* **2008**, *47*, 2089–2097.

(7) Latturner, S. E.; Kanatzidis, M. G. *Inorg. Chem.* **2004**, *43*, 2–4.

(8) Sheldrick, G. M. *SAINT*, version 4; Siemens Analytical X-ray Instruments, Inc.: Madison, WI. Sheldrick, G. M. *SADABS*; University of Göttingen: Göttingen, Germany.

(9) Sheldrick, G. M. *SHELXTL. Structure Determination Programs*, Version 5.0; Siemens Analytical X-ray Instruments, Inc.: Madison, WI, 1995.

(10) (a) Hohenberg, P.; Kohn, W. *Phys. Rev.* **1964**, *136*, B864. (b) Kohn, W.; Sham, L. *Phys. Rev.* **1965**, *140*, A1133. (c) Singh, D. *Planewaves, Pseudopotentials, and the LAPW method*; Kluwer Academic: Boston, 1994.

(11) Blaha, P.; Schwarz, K.; Luitz, J. *WIEN97, a Full potential Linearized Augmented Planewave Package for calculating crystal properties*; Karlheinz Schwarz, Techn. Universität Wien: Austria, 1999.

Table 1. XRD Data Collection Parameters for Some Representative Compounds

	$Eu_3Au_{7.1}Al_{25.9}Hf$	$Ca_3Au_{7.1}Al_{25.7}Nb$	$Yb_3Au_{6.8}Al_{25.8}V$
formula weight (g/mol)	2765.61	2194.91	2605.52
space group	$Pm\bar{3}m$		
a (Å)	8.7429(6)	8.6606(3)	8.6145(10)
V (Å^3)	668.29(8)	649.60(4)	639.28(13)
d_{calc} (g/cm^3)	6.872	5.611	6.768
temperature (K)	290	290	290
radiation	Mo Kα	Mo Kα	Mo Kα
$2\theta_{max}$	73.96	56.25	74.84
index ranges	$-14 \le h, k, l \le 14$	$-11 \le h, k, l \le 11$	$-14 \le h, k, l \le 14$
reflections collected	10224	6133	10293
unique data/parameters	374/21	202/21	370/21
μ (mm^{-1})	51.525	38.455	50.934
R1/wR2 [$I > 2\sigma(I)$]	0.0231/0.0454	0.0257/0.0557	0.0258/0.0447
R1/wR2 (all data)	0.0359/0.0481	0.0272/0.0561	0.0443/0.0490
residual peak, hole (e/Å^3)	2.432, −1.926	1.334, −1.707	1.812, −2.400

Table 2. Atomic Positions and Occupancies for a Few Representative Compounds: (1) $Eu_3Au_{7.1}Al_{25.9}Hf$, (2) $Ca_3Au_{7.1}Al_{25.7}Nb$, and (3) $Yb_3Au_{6.8}Al_{25.8}V$

atom		Wyckoff site	x	y	z	occ		U_{eq}[a]
R	1 Eu	3*d*	0.5	0	0	1	1	0.0083(2)
	2 Ca						2	0.015(1)
	3 Yb						3	0.0107(2)
T	1 Hf	1*b*	0.5	0.5	0.5	1	1	0.0025(2)
	2 Nb						2	0.0026(8)
	3 V						3	0.0043(6)
Au(1)	1	1*a*	0	0	0	0.994(9)	1	0.0209(4)
	2					0.74(1)	2	0.0124(7)
	3					0.560(9)	3	0.0164(7)
Al(1)	1	8*g*	0.1743(2)	*x*	*x*	1	1	0.0117(5)
	2		0.1728(3)				2	0.0064(8)
	3		0.1702(2)				3	0.0071(5)
Au(2)	1	12*i*	0	0.33786(8)	*x*	0.512(3)	1	0.0068(2)
	2			0.3353(1)		0.528(7)	2	0.0084(3)
	3			0.3364(1)		0.519(4)	3	0.0077(2)
Al(2)	1	12*i*	0	0.3652(6)	*x*	0.488(3)	1	0.007(2)
	2			0.3675(9)		0.472(2)	2	0.004(3)
	3			0.3647(7)		0.481(4)	3	0.007(2)
Al(3)	1	12*j*	0.5	0.2687(1)	*y*	1	1	0.0071(3)
	2			0.2704(3)			2	0.0064(8)
	3			0.2721(2)			3	0.0076(4)

[a] U_{eq} is defined as 1/3 of the trace of the orthogonalized U_{ij} tensor.

Table 3. Bond Lengths (in Angstroms) for a Few Representative Compounds

bond	$Eu_3Au_{7.1}Al_{25.9}Hf$	$Ca_3Au_{7.1}Al_{25.7}Nb$	$Yb_3Au_{6.8}Al_{25.8}V$
T−Al(3)	2.860(2) × 12	2.812(3) × 12	2.777(2) × 12
Au(1)−Al(1)	2.639(3) × 8	2.592(4) × 8	2.539(3) × 8
Au(2)−Al(2)	2.607(5) × 2	2.589(8) × 2	2.586(6) × 2
R−Au(2)	3.2764(4) × 4	3.2355(6) × 4	3.2226(6) × 4
R−Al(2)	3.404(3) × 4	3.383(5) × 4	3.351(4) × 4
R−Al(3)	3.322(2) × 4	3.312(3) × 4	3.314(2) × 4

split sites and partial occupancies, the ordered $Fm\bar{3}m$ supercell model was used, and complete occupancy of the stuffed site was assumed (vide infra). For the exchange and correlation parts of the potential the Perdew−Burke−Ernzerhof model was used, which incorporates a generalized gradient approximation (GGA).[12] The atomic radii values (in atomic units, 1 au = 0.529 Å) used in the calculations are as follows: 2.5 au for ytterbium, 2.5 au for gold, 2.3 au for aluminum, and 2.2 au for vanadium. Self-consistent iterations were performed with 28 *k* points in the reduced Brillouin zone with a cutoff between valence and core states of −6.0 Ry; convergence was assumed when the total energy difference between cycles was within 0.0001 Ry. Scalar relativistic corrections were included, and spin−orbit interaction was incorporated using a second variational procedure.[13]

Results and Discussion

The first of these compounds to be isolated in our work was produced serendipitously. $Yb_3Au_{6.8}Al_{26}Ti$ resulted from the inadvertent reduction of titania cement in a crucible containing an aluminum flux reaction intended to form $YbAu_3Al_7$.[4c,7] Reactions with different early transition metals and different rare earths/alkaline earths were carried out to investigate the prevalence of this structure. Surprisingly, this produced a large number of analogues not only with Ti but with a wide variety of early transition metals (see Table 4). Careful analysis of the structure and modifications to the reactant ratio indicate the crucial role of the early transition metal in forming these phases.

Synthesis. The $R_3Au_{6+x}Al_{26}T$ compounds grow from aluminum flux as spheroid crystals which are stable to air and water but dissolve in acids. The calcium containing reactions showed some attack on the fused silica tube because of the volatility of this element at elevated temperatures. The yields for the Sr and Eu analogues ranged from 30−50%

(12) Perdew, J. P.; Burke, K.; Ernzerhof, M. *Phys. Rev. Lett.* **1996**, *77*, 3865.

(13) Koelling, D. D.; Harmon, B. *J. Phys. C* **1980**, *13*, 6147.

Table 4. List of Cell Parameters, Occupancies of the Stuffed Site Au(1) and the Split Site Au(2), and *R*-Values for All Single Crystal Studies[a]

compound	unit cell (Å)	Au(1) occupancy	Au(2) occupancy	R_1/wR_2
$Eu_3Au_{7.1}Al_{25.9}Hf$	8.7429(6)	0.994(9)	0.512(4)	0.0231/0.0454
$Sr_3Au_{7.4}Al_{25.6}Ti$	8.7367(6)	0.990(8)	0.532(4)	0.0237/0.0435
$Eu_3Au_{7.4}Al_{25.6}Zr$	8.729(1)	1.01(1)	0.530(5)	0.0334/0.0393
$Sr_3Au_{7.7}Al_{25.3}Nb$	8.7168(9)	1.000(6)	0.556(6)	0.0289/0.0536
$Eu_3Au_{7.3}Al_{25.7}Ti$	8.7094(5)	0.98(1)	0.522(5)	0.0293/0.0493
$Ca_3Au_{7.4}Al_{25.6}Zr$	8.7090(5)	1.008(7)	0.533(4)	0.0206/0.0381
$Ca_3Au_{7.4}Al_{25.6}Hf$	8.7005(4)	0.997(8)	0.535(8)	0.0345/0.0627
$Yb_3Au_{7.9}Al_{25.1}Zr$	8.6903(5)	0.980(7)	0.574(4)	0.0213/0.0443
$Sr_3Au_{7.7}Al_{25.3}Mn$	8.6851(7)	0.964(9)	0.562(5)	0.0230/0.0502
$Yb_3Au_{7.8}Al_{25.2}Hf$	8.6834(8)	0.99(1)	0.571(5)	0.0261/0.0530
$Eu_3Au_{7.0}Al_{25.9}V$	8.6775(6)	0.875(9)	0.509(5)	0.0255/0.0571
$Ca_3Au_{6.9}Al_{25.9}Ti$	8.6631(5)	0.80(1)	0.510(8)	0.0357/0.0809
$Eu_3Au_{7.2}Al_{25.7}Mn$	8.6623(6)	0.917(8)	0.521(4)	0.0221/0.0418
$Ca_3Au_{7.1}Al_{25.7}Nb$	8.6606(3)	0.74(1)	0.528(7)	0.0257/0.0557
$Yb_3Au_{7.2}Al_{25.6}Nb$	8.6552(4)	0.84(1)	0.532(5)	0.0294/0.0516
$Yb_3Au_{7.0}Al_{25.8}Ti$	8.6509(6)	0.844(7)	0.516(4)	0.0222/0.0463
$Eu_3Au_{6.6}Al_{26.0}Cr$	8.6433(5)	0.542(9)	0.504(5)	0.0309/0.0623
$Ca_3Au_{6.6}Al_{25.9}V$	8.635(1)	0.55(1)	0.508(9)	0.0336/0.0689
$Yb_3Au_{6.6}Al_{25.8}Ta$	8.6290(9)	0.46(1)	0.514(6)	0.0329/0.0706
$Yb_3Au_{6.8}Al_{25.8}V$	8.6145(10)	0.560(9)	0.519(4)	0.0258/0.0447
$Ca_3Au_{7.5}Al_{24.9}Mo$	8.6056(3)	0.332(4)	0.549(4)	0.0185/0.0373
$Ca_3Au_{7.3}Al_{25.0}W$	8.6047(7)	0.313(6)	0.544(4)	0.0191/0.0337
$Eu_3Au_{7.1}Al_{24.9}Re$	8.5836(6)	0.005(6)	0.509(2)	0.0178/0.0319
$Ca_3Au_{5.9}Al_{26.1}Cr$	8.5768(3)	0.008(6)	0.490(6)	0.0242/0.0591
$Yb_3Au_{6+x}Al_{26}Mo$	8.572(1)			problems
$Yb_3Au_{6+x}Al_{26}W$	8.569(1)			problems
$Yb_3Au_{6+x}Al_{26}Cr$	8.5637(9)			problems
$Yb_3Au_{6+x}Al_{26}Mn$	8.552(1)			problems
$Ca_3Au_{6+x}Al_{26}Mn$	8.5400(5)			problems
$Yb_3Au_{6+x}Al_{26}Re$	8.5390(7)			problems
$Ca_3Au_{6+x}Al_{26}Re$	8.5385(5)			problems
$Sr_3Au_{6+x}Al_{26}Zr$	8.765(2)			unit cell only
$Sr_3Au_{6+x}Al_{26}Hf$	8.760(1)			unit cell only
$Sr_3Au_{6+x}Al_{26}Ta$	8.727(2)			unit cell only
$Sr_3Au_{6+x}Al_{26}V$	8.707(2)			unit cell only
$Sr_3Au_{6+x}Al_{26}Mo$	8.700(2)			unit cell only
$Sr_3Au_{6+x}Al_{26}W$	8.693(2)			unit cell only
$Sr_3Au_{6+x}Al_{26}Cr$	8.692(3)			unit cell only
$Eu_3Au_{6+x}Al_{26}Nb$	8.691(6)			unit cell only
$Eu_3Au_{6+x}Al_{26}Ta$	8.684(2)			unit cell only
$Sr_3Au_{6+x}Al_{26}Re$	8.636(1)			unit cell only
$Eu_3Au_{6+x}Al_{26}Mo$	8.631(2)			unit cell only
$Eu_3Au_{6+x}Al_{26}W$	8.629(2)			unit cell only

[a] Listed in order of decreasing unit cell size. Problematic data sets result from compounds with small unit cells (see text). Compounds characterized only by determination of unit cell size are listed at the bottom of the table.

(based on mass of the product and Au as limiting reagent), with higher yields and bigger crystals for the compounds with lighter early transition metals such as Ti, V, and Zr. The yields for the Yb and Ca analogues were lowered to around 20−40% by the competing formation of $YbAu_3Al_7$ and the previously unknown but isostructural $CaAu_3Al_7$ ($R\bar{3}c$, $a = 8.047(2)$Å, $c = 21.247(7)$Å). Formation of the ternary phases was particularly prevalent in reactions with more refractory early transition metals such as Ta and W; $Ca_3Au_{6+x}Al_{26}Ta$ could not be isolated. It is possible that more reactive forms of these elements, perhaps in finely divided oxide powder form (such as $Ca_2Ta_2O_7$ or $CaWO_4$, which would be reduced in the aluminum flux medium)[14] would allow for better incorporation of these refractory metals into the products. Yields were also tied to the size of the unit cell edge, with smaller unit cells being less stable than larger ones (and therefore forming in lower yield; vide infra). Byproducts of the reactions include recrystallized gold, small amounts of $BaAl_4$ type $RAuAl_3$ for R = Eu and Ca, and binary aluminides of the early transition metals (such as $TiAl_3$).

Structural Characteristics. All of the $R_3Au_{6+x}Al_{26}T$ compounds form in the cubic $Pm\bar{3}m$ space group. The structure of these materials, shown in Figure 1, can be described as a stuffed variant of the $BaHg_{11}$ type. The R atoms (Ca, Sr, Eu, Yb) occupy the barium positions of the parent structure, and the other atoms occupy the mercury positions; one position that is vacant in the $BaHg_{11}$ structure is occupied by a gold atom (the stuffed site). The 1*b* Wyckoff site at the center of the unit cell is occupied by an early transition metal atom coordinated by a cuboctahedron of neighboring aluminum sites (Al(3), Wyckoff site 12*j*). This coordination environment is a common structural motif in early transition metal aluminides such as $TiAl_3$ and $ZrAl_3$.[15] This suggests that the presence of early transition metals in aluminum fluxes might form cuboctahedral "seed clusters" that template the formation of the cubic $R_3Au_{6+x}Al_{26}T$

(14) Aluminum flux is an excellent reducing agent; a combination of the perovskite SrTiO3 and Au in excess aluminum produces $Sr_3Au_7Al_{26}Ti$ (ref 7); aluminum flux is also sufficiently aggressive to reduce the refractory oxide ThO_2 (ref 6a).

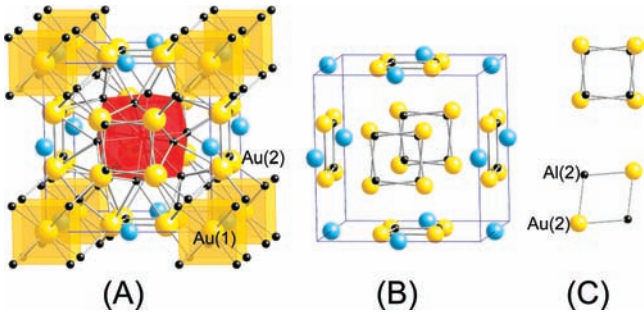

Figure 1. Structure of cubic $R_3Au_{6+x}Al_{26}T$. (a) The unit cell, with coordination environments around the stuffed site Au(1) (yellow) and the transition metal T (red) shown in polyhedral mode. Blue spheres represent R atoms; small black spheres are Al atoms. (b) The $AuAl_8$ cubes and TAl_{12} cuboctahedra have been removed to highlight the Au(2)/Al(2) split site. (c) The 50% occupancy of the Au(2) and Al(2) sites results in an Al_2Au_2 rhombus with strong Au−Al bonding.

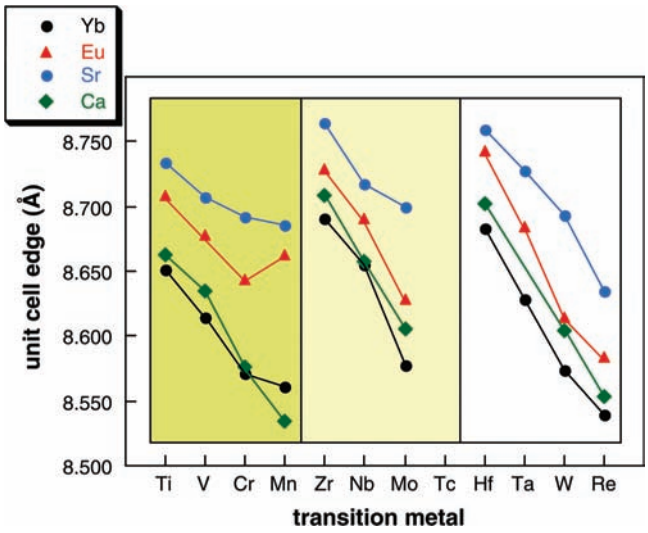

Figure 2. Unit cell sizes of the $R_3Au_{6+x}Al_{26}T$ phases, showing their dependence on R and T.

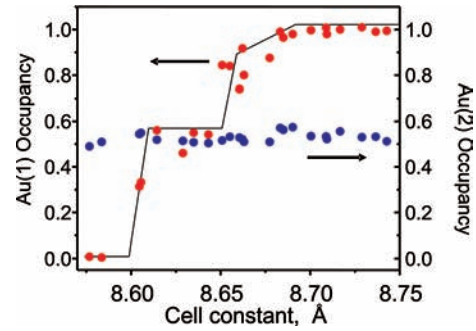

Figure 3. Occupancy variation of the Au(1) and Au(2) sites of $R_3Au_{6+x}Al_{26}T$ phases with unit cell constant.

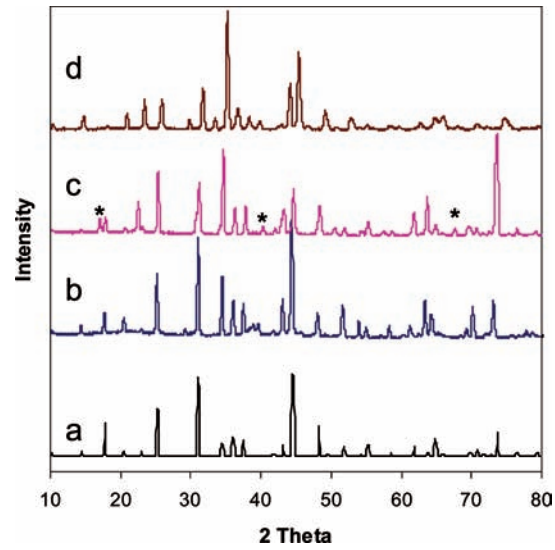

Figure 4. Powder XRD patterns of $R_3Au_{6+x}Al_{26}T$ analogues. (a) Calculated pattern for the disordered $Sr_3Au_{6+x}Al_{26}Ti$ $Pm\bar{3}m$ cell. (b) Observed pattern for $Sr_3Au_{6+x}Al_{26}Nb$. (c) Observed pattern for $Ca_3Au_{6+x}Al_{26}Ti$, with $Fm\bar{3}m$ supercell peaks marked with asterisks. (d) Observed pattern for $Yb_3Au_{6+x}Al_{26}Mn$. The relatively broad peaks at high 2θ values are indicative of the increased amount of short-range disorder for this small unit cell.

structure. All early transition metals in groups 4−7 (from Ti to Re) can be incorporated into the 1*b* site. Reactions with members of groups 3 (Sc, Y, La) and 8 (Fe, Ru, Os) did not form this structure, in agreement with the fact that these transition metals favor different coordination environments in their binary aluminides. As shown in Figure 2, the cell edges vary in a regular fashion with the size of the early transition metal T and with the size of the R element.

The 1*a* Wyckoff site is located in the center of a cube of eight Al(1) aluminum atoms; this site is not occupied in the parent structure of $BaHg_{11}$. A gold atom occupies this site in the title compounds; $R_3Au_{6+x}Al_{26}T$ can therefore be described as a stuffed variant of $BaHg_{11}$, where *x* indicates the extent of stuffed site filling. Gold-centered Al_8 cubes are a feature of the binary antifluorite structure $AuAl_2$ phase and have also been observed in multinary intermetallics such as $Th_2Au_3Al_4Si_2$ and $YbAu_4Al_8Si$.[6] $R_3Au_7Al_{26}T$ compounds with fully occupied stuffed sites feature Au(1)−Al(1) bond lengths of 2.59−2.63Å; the observed Au−Al bond length in bulk $AuAl_2$is within this range (2.597Å).

The filling of this site in these compounds shows a strong correlation with unit cell size; this is highlighted in Table 4, which lists the gold site occupancy parameters for the compounds in order of decreasing unit size. Larger unit cells (above 8.68 Å, such as that of $Sr_3Au_7Al_{26}Ti$) show full occupancy of this site by gold. Unit cells in the range 8.65−8.68Å show occupancies between 70−90%; for smaller unit cells in the range 8.61−8.65Å the occupancy drops to 45−55%. It is expected that the amount of gold in the stuffed site should fall as the unit cell shrinks, since placing a gold atom into an Al_8 cube that is too small to allow for suitable Au−Al bond distances will produce local distortions and lattice strain, an energetically unfavorable situation. However, the dependency of Au(1) occupancy on unit cell size is not gradual or linear. Instead, the occupancy drops in distinct steps, which are apparent in Table 4 and Figure 3. The reason for this is not clear at this time.

Below a cell edge of around 8.60 Å, the yield and crystallinity of the products drops drastically. While single crystal X-ray diffraction (XRD) data for compounds such

(15) Villars, P. Pearson's Handbook, Desk Edition. *Crystallographic Data for Intermetallic Phases*; ASM International: Materials Park, OH, 1997.

as $Ca_3Au_{6+x}Al_{26}Mo$ can be refined, there is additional disorder in the structure (the Al(1) site is split and/or mixed). The Au(1) site occupancy is under 30%. For compounds with a cell edge smaller than around 8.575 Å, the data can be indexed to a $Pm\bar{3}m$ cell, but the structure could not be solved satisfactorily. The data showed high R(int) values and the R_1 value remained above 0.10 even when the $BaHg_{11}$ structure is put in as the starting model. The structure solution indicated partial occupancies on most of the sites and unreasonable bond lengths. Powder diffraction of such samples—on powder ground from what appear to be well-formed, facetted crystals—showed the expected $Pm\bar{3}m$ pattern, but the high angle reflections were broad, as shown in Figure 4. Presumably, the atomic arrangement is not entirely stable below a certain unit cell size, needing to incorporate a large amount of local disorder to form the extended $BaHg_{11}$ structure. Similar characteristics (long-range order accompanied by short-range disorder) are found in aluminide quasicrystals and quasicrystal approximants.[2]

Some of this local disorder may be embodied in the observed splitting of the 12*i* Wyckoff site, which allows for occupancy of this site by a mixture of Al and Au. The two positions resulting from the splitting are also 12*i* sites. One is roughly 50% occupied by gold (Au(2)); the other is 50% occupied by aluminum Al(2). The occupancies of the Au(2) and Al(2) sites were allowed to vary while being restrained to sum to 1; occupancies refined to around 50% for most of the compounds, with a slight enrichment of gold seen for some analogues. These small deviations from half-occupancy result in variation from the idealized formula $R_3Au_{6+x}Al_{26}T$; the resulting $R_3Au_{(6+y)+x}Al_{26-y}T$ stoichiometries are found in Table 4. A possible reason for the splitting of this site is to allow the formation of suitable bond lengths between the aluminum or gold atoms and the neighboring R atom. It also allows for Al−Au bonds of an appropriate length between adjacent split sites (see Figure 1). In essence, this produces an Au_2Al_2 rhombus with strong Au−Al bonds similar to that found in bulk $AuAl_2$ (2.57−2.66Å in length; see Table 3) instead of Al_4 or Au_4 squares with bond lengths that are unreasonable.

The disorder in rhombus orientation resulting from this splitting is averaged over the crystal, resulting in $Pm\bar{3}m$ symmetry. Some evidence of ordering of the split site to form an $Fm\bar{3}m$ cell with a doubled unit cell edge was observed in several of the $Ca_3Au_{6+x}Al_{26}T$ analogues. This includes some additional reflections in the single crystal data corresponding to a doubled F-centered cell, and weak superstructure peaks in the powder XRD pattern (Figure 4). However, the extent of ordering was not complete enough in any of the analogues to solve the single crystal structure in the $Fm\bar{3}m$ supercell.

While it might appear that early transition metals promote entirely different structures than silicon when these elements are incorporated into a molten aluminum solution containing rare earth elements and gold, some similarities in the products are evident. RE/Au/Al/Si mixtures result in a series of compounds $(RE[AuAl_2]_nAl_2(Au_xSi_{1-x})_2$, where $n = 0-3)$ which can be viewed as intergrowths of $BaAl_4$ type layers containing the rare earth atoms, and antifluorite type $AuAl_2$

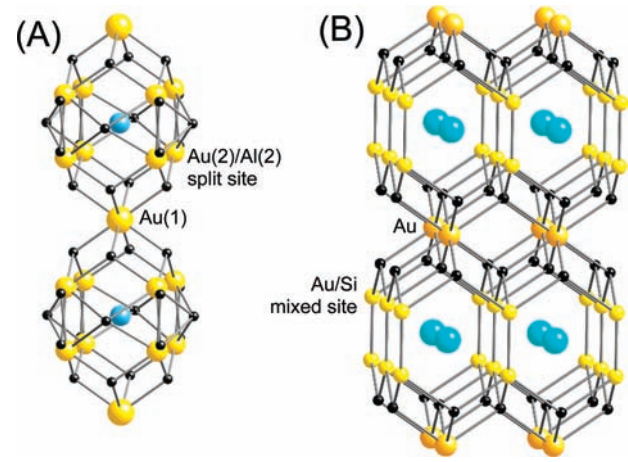

Figure 5. Comparison between the local coordination environments of rare earth/alkaline earth atoms (blue spheres) in (A) the $R_3Au_{6+x}Al_{26}T$ structure and (B) the $BaAl_4$-related tetragonal $REAu_2Al_4Si$ structure. Small black spheres represent aluminum atoms; yellow spheres represent gold sites or mixed sites as indicated.

slabs of varying thickness.[6] Upon inspection of the local environment of the rare earth/alkaline earth R atoms in the cubic $R_3Au_{6+x}Al_{26}T$ structure, it is evident that the coordination is very similar to the $BaAl_4$-type cage observed in the silicides (the local environments are compared in Figure 5). The R atom sites are coordinated in a roughly cubic fashion to mixed occupancy sites containing a mixture of gold and aluminum (Au and Si in the silicides). This is in agreement with electronegativity concepts that support the electropositive elements being closely coordinated by the most electronegative elements in the compounds.

Therefore, it appears that the largest difference in the behavior of Si and early transition metals in R/Au/aluminum flux reactions is in directing the packing of these $BaAl_4$-like units. Silicon appears to act as a stable "capping" agent on the face of large $AuAl_2$ slabs, resulting in a series of structures featuring such 2-D antifluorite units. Early transition metals, on the other hand, favor a high symmetry coordination sphere of aluminum atoms. As mentioned previously, a large number of binary aluminides feature the early transition metals surrounded by 12 Al atoms in a cuboctahedral MAl_{12} arrangement. Icosahedral MAl_{12} units are also prevalent in binary and ternary phases such as WAl_{12} and RT_2Al_{20}, as well as icosahedral quasicrystalline approximants.[16] MAl_{12} icosahedral clusters may also form as the reaction progresses, but interconversion between icosahedral and cuboctahedral geometry is relatively simple, and the molten medium allows for cluster fluxionality.[17] The formation of a cuboctahedral TAl_{12} unit within the reaction mixture may promote the organization of the $BaAl_4$-like rare earth containing building blocks into the cubic $R_3Au_{6+x}Al_{26}T$ structure.

Reports in the literature support the idea of early transition metals being a template for the $BaHg_{11}$ structure type.

(16) (a) Niemann, S.; Jeitschko, W. *J. Solid State Chem.* **1995**, *114*, 337–341. (b) Wolff, M. W.; Niemann, S.; Ebel, T.; Jeitschko, W. *J. Magn. Magn. Mater.* **2001**, *223*, 1–15.

(17) (a) Yi, J. Y.; Oh, D. J.; Bernholc, J.; Car, R. *Chem. Phys. Lett.* **1990**, *174*, 461–466. (b) Carlsson, A. E. *Phys. Rev. B* **1991**, *43*, 12176–12186.

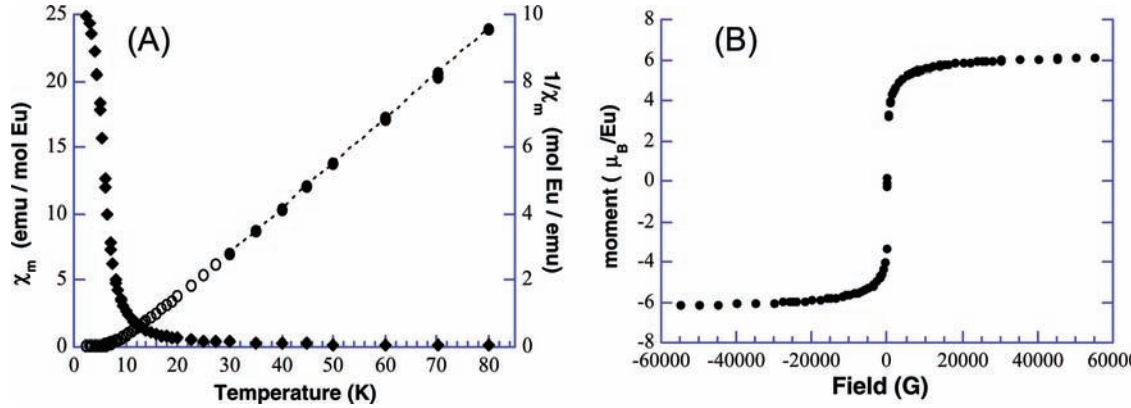

Figure 6. (a) Temperature dependence of the magnetic susceptibility of $Eu_3Au_{6+x}Al_{26}Zr$ showing Curie−Weiss behavior at high temperatures and a ferromagnetic transition at 10 K. (b) The field dependence of the magnetic susceptibility of $Eu_3Au_{6+x}Al_{26}Zr$ measured at 3 K, showing ferromagnetic saturation above 5000 G.

Gladyshevskii et al. reported the formation of $Y_3Ni_{6.5}Al_{26}Ta$ when an arc melted sample of YNi_2Al_9 was annealed in tantalum foil at high temperature.[18] $Ce_3Cu_8Al_{24}Mn$ was reported to form in a heat-resistant aluminum alloy containing Ce, Cu, and Mn, although the siting of these elements in the structure was not specified.[19] Initial work in our laboratory on the growth of palladium compounds from aluminum flux has produced $RE_3Pd_{6+x}Al_{26}T$ with RE = Ce, Nd, and Gd, and T = Ti and Zr and will be reported elsewhere.

On the other hand, there have been a number of literature accounts of ternary aluminide phases—with no early transition metal—reported to have the $BaHg_{11}$ structure. These include reports of $YbAg_4Al_7$ and $CeAg_3Al_8$.[20] However, the report on the Yb compound states that it was synthesized by heating elemental reactants at high temperatures in a molybdenum crucible. (Synthetic details on the cerium compound were not reported, but the work was carried out by the same group.) Molten aluminum and aluminum-rich mixtures will attack refractory metals at high temperatures, as demonstrated by the affinity for tantalum foil shown by YNi_2Al_9.[18] It is therefore possible that the reported ternary products of the $BaHg_{11}$-type are actually quaternary compounds containing additional elements such as for example $Yb_3Ag_{12}Al_{20}Mo$. The early transition metal is only one atom in a very large unit cell of 35 atoms and easily missed in elemental analysis.

To test this hypothesis, we attempted aluminum flux syntheses of (Ce or Yb)/Ag/Al ternary compounds using cast alumina crucibles to avoid the possibility of contamination. Reactants were combined in a 1:2:15 molar ratio, prepared and heated as described for the title compounds. The reaction containing cerium produced $CeAgAl_3$ ($BaAl_4$ structure type: *I4/mmm*, $a = 4.320(2)$ Å, $c = 11.043(5)$ Å). The ytterbium reaction produced $Yb_8Ag_{17}Al_{49}$ ($Yb_8Cu_{17}Al_{49}$ structure type, *I4/mmm*, $a = 8.886(1)$ Å, $c = 16.667(2)$ Å). No ternary variants of the $BaHg_{11}$ structure type were obtained. However, when the reactions were modified by addition of a refractory metal (Ta or Mo, to mimic the presence of a metal crucible), quaternary phases were produced, including the $BaHg_{11}$ type $Ce_3Ag_{6+x}Al_{26}Ta$ ($Pm\bar{3}m$, $a = 8.677$Å). It is likely that silver will show the same tendency exhibited by gold and palladium to form $R_3M_{6+x}Al_{26}T$ phases with a variety of electropositive elements (such as R = Yb, Ce, Ca) and a wide range of early transition metals T.

Magnetic Properties. Varying the early transition metal has little effect on the magnetic properties of $R_3Au_{6+x}Al_{26}T$ phases, which are instead determined by the rare earth/alkaline earth element R. The Ca and Sr analogues show Pauli paramagnetic behavior, with a temperature independent paramagnetism in the range 10^{-3} emu/mol. The $Eu_3Au_{6+x}Al_{26}T$ compounds all show Curie−Weiss behavior at high temperature; the fit of the inverse susceptibility indicates Eu is divalent in all the analogues tested. A sharp increase in the susceptibility is observed at 10 K (see Figure 6), indicative of a ferromagnetic transition. Ferromagnetic ordering is also evidenced by the magnetization data taken at 3 K, which shows a saturation of magnetization at fields above 5000 G. The saturation value is around 6 μ_B/Eu ion, which is roughly 75% of the theoretical maximum for Eu^{2+} (7.94 μ_B/Eu); this is commonly observed in isotropic powder samples.[21] No hysteresis was observed indicating that the $Eu_3Au_{6+x}Al_{26}T$ compounds are soft magnets.

The $Yb_3Au_{6+x}Al_{26}T$ compounds have more complex magnetic behavior, with the Yb ions showing two kinds of non-integral (Yb^{2+}/Yb^{3+}) valence. All the ytterbium analogues tested (with T = Ti, V, Mn, Cr, Mo, Ta, Re) have susceptibility data similar to that of the Ti analogue reported previously; three representative data sets are shown in Figure 7.[6] Above 100 K, the inverse susceptibility follows the Curie−Weiss law, indicating that the Yb valence is constant with temperature. The fit of the data results in a moment per Yb in the range of 1.5−2 μ_B, between the theoretical values of 0 μ_B (Yb^{2+}) and 4.1 μ_B (Yb^{3+}). There is only one crystallographic Yb site, but the local environment around this Yb site varies from cell to cell because of the nearby

(18) Gladyshevskii, R. E.; Cenzual, K. *J. Alloys Cmpd.* **1996**, *240*, 266–271.
(19) Zarechnyuk, O.; Kripyakevich, P.; Cherkashin, E.; Kolobnev, I. *Inorg. Mater.* **1967**, *3*, 153.
(20) (a) Cordier, G.; Korsam, G.; Kniep, R. *J. Magn. Magn. Mater.* **1988**, *76−77*, 653–654. (b) Schank, C.; Cordier, G.; Kniep, R.; Steglich, F. *J. Alloys Cmpd.* **1994**, *207/208*, 333–336.
(21) Kittel, C. *Introduction to Solid State Physics*, 6th ed.; John Wiley and Sons, Inc.: New York, 1986.

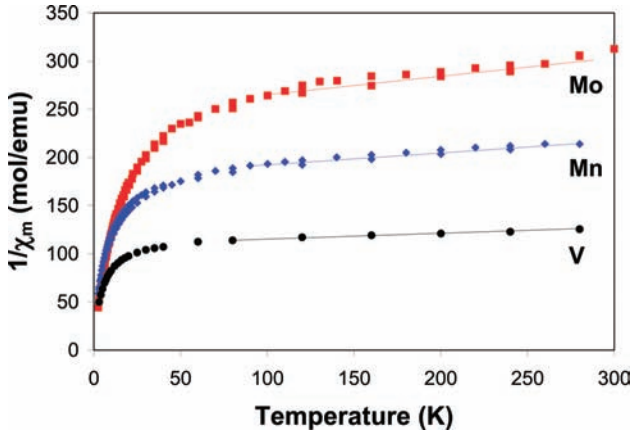

Figure 7. Temperature dependence of the inverse susceptibility of three $Yb_3Au_{6+x}Al_{26}T$ compounds (T = V, Mn, Mo). The dashed lines represent the linear regions fit to the Curie−Weiss law. Below this temperature region, the samples show Yb^{2+}/Yb^{3+} fluctuating valence.

disordered Au/Al split site. The coordination of Yb by the Au2/Al2 split site is shown in Figure 5. This causes the valence of Yb to vary from cell to cell, resulting in an apparent non-integral valence, a state referred to as *inhomogeneous valence*. A similar effect has been observed in other disordered compounds. For instance, the random distribution of boron atoms on interstitial sites in $EuPd_3B$ results in varying local coordination around the single europium site in this structure; Mössbauer studies show the presence of both Eu^{2+} and Eu^{3+}.[22] Another example is found in $YbPd_xGa_{11-x}$, which is a $BaHg_{11}$ analogue (synthesized in a Ta crucible, which might be incorporated) possessing Pd/Ga mixed sites adjacent to the Yb site. Susceptibility measurements indicate an average valence of 1.9 μ_B, and X-ray absorption spectroscopy reveals the presence of both Yb^{2+} and Yb^{3+} in the material.[23]

The linear inverse susceptibility of $Yb_3Au_{6+x}Al_{26}T$ at high temperatures indicates that while the ytterbium valence may be inhomogeneous, it does not change with temperature. However, $1/\chi_m$ becomes non-linear below 100 K, suggesting incipient temperature dependence of the valence. This state of *fluctuating valence* often results in compounds that have rare earth f-bands in close proximity to the Fermi level.[24] As the temperature changes, the f-band can cross E_f and promote its electrons to the conduction band. To investigate this, band structure calculations were carried out on an Yb-containing model structure.

Band Structure Calculations. The $Fm\bar{3}m$ supercell model of $Yb_3Au_7Al_{26}V$ was used as the archetypal ordered compound for band structure calculations; complete occupancy of the stuffed site was assumed. The total density of states (DOS) and partial DOS for several individual atoms are shown in Figures 8 and 9. The total DOS is dominated by the f-orbitals of Yb, forming the very narrow bands at −0.3 and −1.7 eV below the Fermi level. The close vicinity of the former band to E_f is what facilitates the temperature dependence of the ytterbium valence that is observed at low temperatures. Another distinctive feature in the total DOS are the bands between −5 and −9 eV below E_f, which correspond to the filled d-orbitals of the gold atoms in the structure. Filled and stabilized late transition metal d-bands—resulting in diamagnetic behavior for these atoms—are commonly observed in polar intermetallic aluminides.[25] This reflects the relatively high electronegativity of the late transition elements compared to that of the rare earth and aluminum metals in these compounds. The more electropositive elements will donate electrons to the late transition metals, filling their d-orbitals.

There is a pseudogap in the $Yb_3Au_7Al_{26}V$ DOS at the Fermi level, which is characteristic of many polar intermetallic compounds. The largest contribution to the DOS at E_f comes from the vanadium d-bands, which are partially filled and cross the Fermi level (Figure 9a). These interact strongly with the p-orbitals on the surrounding Al(3) atoms forming the cuboctahedron (Figure 9b). Similar hybridization between Al-p and V-d orbitals is seen in VAl_3, which also features vanadium surrounded by a cuboctohedron of aluminum atoms. This interaction results in a pseudogap near E_f for this binary compound and is associated with formation of covalent bonds; NMR studies on VAl_3 also evidence covalency in this compound. The strong interaction between vanadium and the surrounding aluminum atoms is hypothesized to stabilize the structure and produce unusual electronic behavior.[26] The stabilization of the TAl_{12} cuboctahedron is also occurring in the quaternary compounds studied here and may also be a factor in producing these cuboctahedra in the flux to template the formation of the $R_3Au_{6+x}Al_{26}T$ phases. The other dominant bands near the Fermi level are formed from the p-orbitals of the aluminum and gold atoms in the compound. The strong interaction between the p-orbitals of the Au(2) and Al(2) atoms that form the rhombi (highlighted in Figure 1) can be seen in the hybridization of their bands, shown in Figure 9c and 9d. These Au_2Al_2 rhombi may also be a strongly stabilizing structural unit.

Conclusions

A remarkably large family of $R_3Au_{6+x}Al_{26}T$ compounds with the $BaHg_{11}$ structure is possibly templated by the early transition metal T. The family is likely even larger if replacements in the Au sites are contemplated. The observed reaction trends in aluminum flux and common structural building blocks seen in the intermetallic products allow postulation about the species that form in this molten medium. The interaction of silicon and gold in this solvent in the presence of rare earth elements is strong and appears to promote the growth of 2-D $AuAl_2$ slabs, driving the formation of layered compounds such as the homologous

(22) Cianchi, L.; DeGennaro, S.; Gulisano, F.; Mancini, M.; Spina, G. *J. Phys.: Condens. Matter* **1991**, *3*, 781–785.
(23) Grin, Y. N.; Hiebl, K.; Rogl, P.; Godart, C.; Alleno, E. *J. Alloys Compd.* **1997**, *252*, 88–92.
(24) Varma, C. M. *Rev. Mod. Phys.* **1976**, *48*, 219–238.
(25) (a) Gout, D.; Benbow, E.; Gourdon, O.; Miller, G. J. *Inorg. Chem.* **2004**, *43*, 4604–4609. (b) Gout, D.; Benbow, E.; Gourdon, O.; Miller, G. J. *J. Solid State Chem.* **2003**, *174*, 471–481. (c) Gout, D.; Barker, T. J.; Gourdon, O.; Miller, G. J. *Chem. Mater.* **2005**, *17*, 3661–3667. (d) Nordell, K. J.; Miller, G. J. *Angew. Chem., Int. Ed. Engl.* **1997**, *36*, 2008–2010.

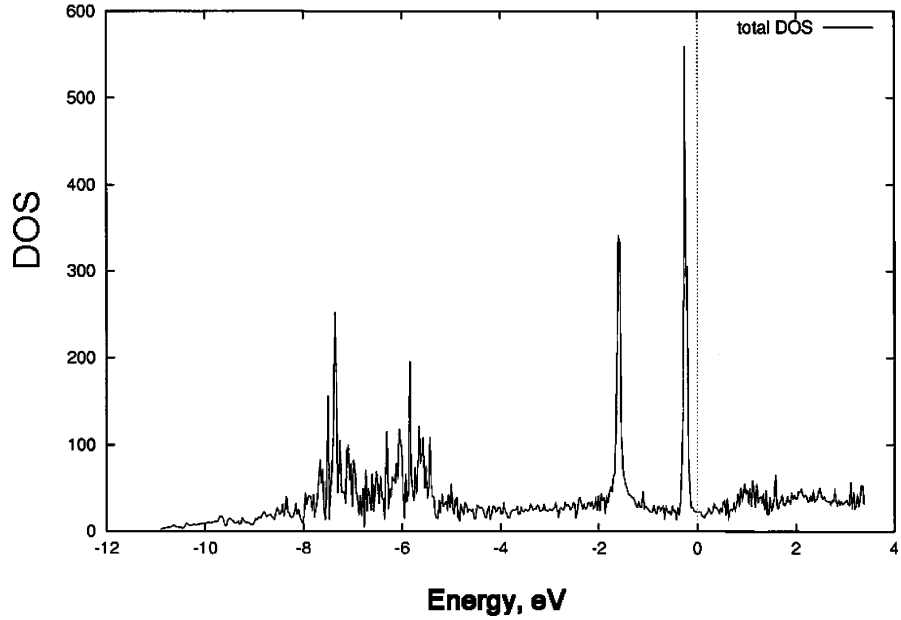

Figure 8. Total DOS for $Yb_3Au_7Al_{26}V$ calculated for the $Fm\bar{3}m$ ordered superstructure of $Yb_3Au_7Al_{26}V$.

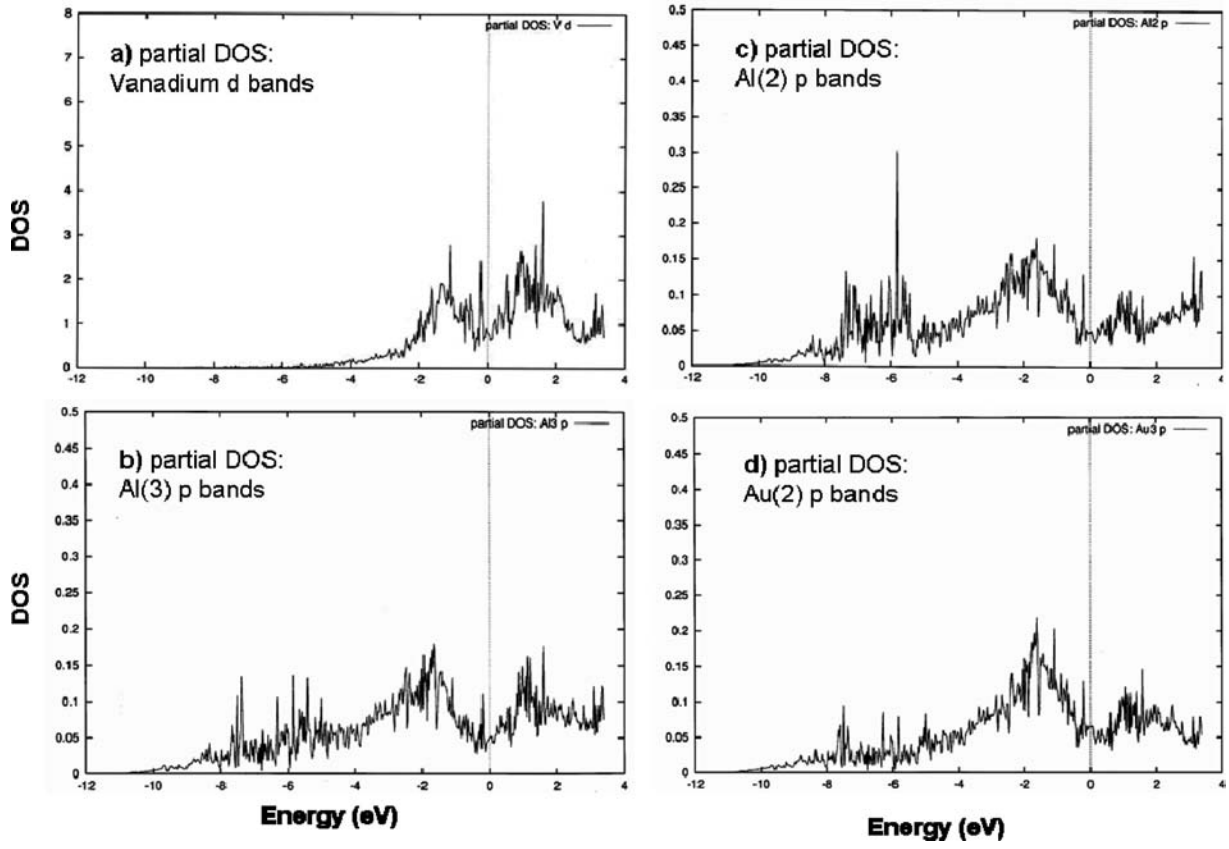

Figure 9. Band structure diagrams calculated for the $Fm\bar{3}m$ ordered superstructure of $Yb_3Au_7Al_{26}V$. (a) Partial DOS for the d-orbitals of vanadium. (b) Partial DOS for the p-orbitals of the Al(3) atoms. (c) Partial DOS for the p-orbitals of the Al(2) atoms. (d) Partial DOS for the p-orbitals of the Au(2) atoms.

series $RE[AuAl_2]_nAl_2(Au_xSi_{1-x})_2$. The presence of an early transition metal in the flux may promote formation of a TAl_{12} cuboctahedral cluster, which templates the cubic $BaHg_{11}$ structure. As R and T get smaller, the unit cell size decreases, the occupancy of the stuffed site falls to zero, and the structure becomes increasingly disordered. The many manifestations of disorder in these compounds (leading to intermediate valence in the Yb analogues, to evidence of supercells in the calcium analogues, and in

(26) (a) Krajci, M.; Hafner, J. *J. Phys.: Condens. Matter* **2002**, *14*, 1865–1879. (b) Lue, C. S.; Chepin, S.; Chepin, J.; Ross, J. H. *Phys. Rev. B* **1998**, *57*, 7010–7014.

some cases to difficulty in structure solution) may reflect aspects of the chemistry of aluminum that make this element so dominant in the fields of quasicrystals and bulk metallic glasses.

Finally, because the element T is one of 39 atoms in the formula and it is key to stabilizing the cubic structure, we suspect that it may have easily been missed in older structure determinations of compounds adopting the $BaHg_{11}$ structure. The work reported here has broader implications for many previously described $BaHg_{11}$ structures and calls for a more careful reexamination to check for the presence of early transition metals in the 1*b* site of the structure type.

Acknowledgment. Financial support from the Department of Energy (Grant DE-FG02-07ER46356 Northwestern University) is gratefully acknowledged.

Supporting Information Available: Crystallographic collection parameters and tables of atomic positions, thermal parameters, bond lengths and angles for most analogues are available in CIF format. This material is available free of charge via the Internet at http://pubs.acs.org.

IC801095V